

# Observation-Oriented Design of a Monolithic Piezoelectric Microactuator with Optimally Integrated Sensor.

Roba El Khoury Moussa

CEA, LIST, Ambient Intelligence and Interactive Systems Departement, Fontenay Aux Roses, F-92265, France  
Femto-st Institute, Besançon, France

Mathieu Grossard, Mehdi Boukallel

CEA, LIST, Ambient Intelligence and Interactive Systems Departement, Fontenay Aux Roses, F-92265, France

Nicolas Chaillet, Arnaud Hubert

Femto-st Institute, Besançon, France

## Abstract

This paper presents an evolution in an optimization method, called FlexIn, developed for the optimal design of piezoelectric compliant smart structures. FlexIn is based on a flexible building block method that uses a genetic algorithm approach, to optimize a truss-like planar structure made of piezoelectric passive, active and, with the work reported in this paper, sensitive building blocks. The model of these blocks is established by means of a finite-element electromechanical formulation. The main contribution of this paper is to present a new observation-oriented criterion, along with a static electromechanical one, considered in the optimization procedure for the optimal placement of piezoactuating and piezosensing parts in the compliant micro-structure. In order to underline the interests of such a criterion, performances of three pseudo-optimal piezoelectric smart structures are drawn. Their analysis and comparison illustrate the role of the optimization method and the observation-oriented criterion, in the design of smart structures and in simplifying their control afterwards.

## 1 Introduction

In many robotic applications, the use of compliant smart mechanisms is being widely propagated. In particular, when considering small-scale systems, e.g. for micro-robotic operations like micro or nano-positioning, micro-gripping, etc., there are many advantages of compliant smart mechanisms, such as simplified manufacturing, reduced assembly costs, reduced kinematic noise, high precision, and miniaturization by actuation and sensing functions integration. One type of smart material typically used in compliant structures design is the piezoceramic PZT. An interesting advantage of such material is the reversibility of its electromechanical coupling effect, which explains its potential use in microrobotic applications as actuator and/or sensor [1], [2].

Few studies consider the topology optimization (shape) of monolithic PZT active structures [3] with exteroceptive sensors [4]. Furthermore, a number of papers only address the problem of optimally designing PZT active structures with optimally integrated sensors [5], [6], [7]. In each one of these studies aiming for vibration control, the optimal placements of piezoelectric actuator and sensor on a flexible plate, based on controllability and observability criteria respectively, are achieved separately. The resulting modes' observability and controllability could disagree, thus eliminating the possibility of integrating both smart functions in the structure.

Therefore, we developed two criteria that can help the designer to optimally place the piezoelectric parts simultaneously in the compliant structure. The first one considers purely static electromechanical aspect, i.e. the maximization of the amount of electric charges induced by the piezoelectric sensor's deformation, while the second one is based on modal observability aspects. This last criterion is a useful tool to optimize dynamic operating flexible actuators with integrated piezoelectric sensors, and to ensure their efficient control afterwards. It is based on the structure's balanced-gramian and observability gramian. From these two indicative characteristics, the criterion aims to optimize the observability of the 'k' first modes specified by the designer, under a condition that the control authority of those same modes is highly dominant comparing to the residual ones. Both criteria are integrated in a more global systematic design approach, based on topology optimization of the structure, as well as that of its frequency responses, to design compliant integrated smart micromechanisms. This method is based on the flexible building block method, called FlexIn ("Flexible Innovation") [8] and [4], which uses an evolutionary approach, to optimize a truss-like planar structure including passive, active and now sensitive building blocks made of piezoelectric material.

This paper is organized as follows: we will first briefly review the underlying idea of the FlexIn methodology for the design of smart compliant mechanisms. The electromechanical approach, based on a finite element (FE) formu-

lation, is established for the model of the piezoactuating and piezosensing building blocks. From this computation, the piezosensing model leads to the first static criterion described earlier. In a second part, the state model approach used in FlexIn is presented, where the mechanism is discretized on its modal components. This particular representation simplifies the computation of a gramian-based criterion, taking into account simultaneously, controllability aspects for actuators and observability aspects for sensors in flexible structures. Hence, the two criteria ensure static and dynamic performances, required to optimally synthesize a compliant monolithic microactuator with integrated piezoelectric sensor. Optimization results are presented in the last part. Performance comparisons between three of the obtained pseudo-optimal structures exhibit the interests of the proposed optimization method and observability-oriented criterion, for the design of smart structures.

## 2 FlexIn: A Compliant Smart Mechanisms Stochastic Design Methodology

### 2.1 Principles of the method

FlexIn is an optimization software for the design of planar compliant micromechanisms. It uses a multiobjective genetic algorithm approach, which consists of searching for an optimal distribution of allowed building blocks, chosen in three specific libraries, composed of 36 passive blocks, 19 piezoactuating blocks, and 19 piezosensing blocks, made of beams assembly (Fig. 1). In addition to topological specifications, the optimization problem appoints an optimal set of boundary conditions (fixed frame location, contacts, actuators, sensors, end-effectors, etc.), dimensions and materials, based on the optimization criteria selected by the designer. More detailed descriptions of the method can be found in [8] and [4].

### 2.2 Electromechanical FE model of the piezoelectric structures

In the optimization procedure, the computation of different criteria requires the FE model of each block of the libraries. To obtain the FE formulation of the piezoelectric blocks, a model of a piezoelectric beam is needed first, exploiting both direct and inverse piezoelectricity effects separately for sensing and actuation purposes respectively (Fig. 2). To do so, the compliant mechanism is assumed to undergo structural planar deformation, leading to considering Navier-Bernoulli beams type FEs.

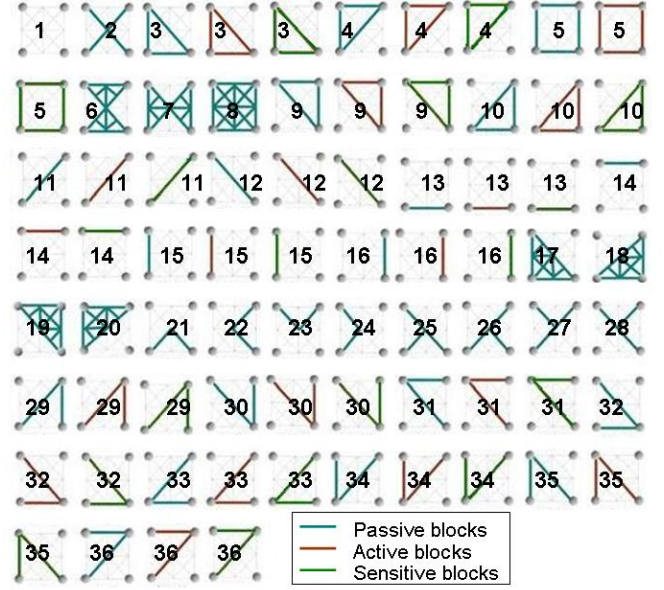


**Figure 1:** Passive (blue), piezoactuating (red) and piezosensing (green) libraries of compliant building blocks, for planar compliant mechanisms synthesis using FlexIn.

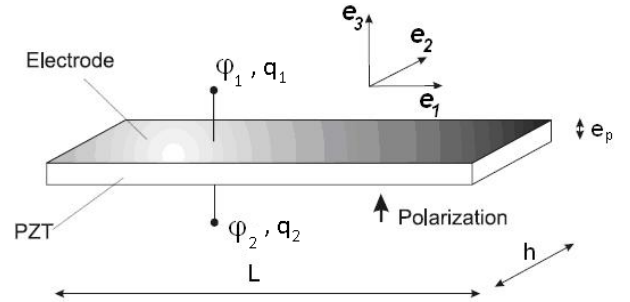


**Figure 2:** Thickness-polarized piezoelectric beam transducer with electroded surfaces, and orientation in the material reference frame ( $\mathbf{e}_1, \mathbf{e}_2, \mathbf{e}_3$ ). ( $\varphi_1, \varphi_2$ ) and ( $q_1, q_2$ ) denote respectively the electric potential for actuation case, and the electric charges for sensing case, of the two electrodes.

#### 2.2.1 FE formulation of the piezoelectric beam

From modified Hamilton's principle for a general electromechanical system [9], piezoelectric beam model is established through two equations representing respectively the actuator and sensor functioning modes, as follow:

$$\begin{aligned} \mathbf{M}_b \ddot{\boldsymbol{\eta}}_b + \mathbf{K}_b \boldsymbol{\eta}_b &= \mathbf{G}_b \boldsymbol{\Phi}_b + \mathbf{F}_r \mathbf{b} \\ \mathbf{q}_b &= \mathbf{G}_b^t \boldsymbol{\eta}_b + \mathbf{C}_b \boldsymbol{\Phi}_b \end{aligned} \quad (1)$$

where  $\boldsymbol{\eta}_b = (u_A, v_A, \omega_A, u_B, v_B, \omega_B)^t_{R_p}$  is the nodal displacement vector in the beam coordinate system  $R_p = (A, \mathbf{x}_p, \mathbf{y}_p, \mathbf{z}_p)$  (see Fig.3).  $\mathbf{M}_b$ ,  $\mathbf{K}_b$ ,  $\mathbf{G}_b$  and  $\mathbf{C}_b$  are respectively, the mass, stiffness, electromechanical coupling and electric capacity beam matrices.  $\boldsymbol{\Phi}_b =$

$[\varphi_1 \varphi_2]^t$  and  $\mathbf{q}_b = [q_1 q_2]^t$  are the vectors representing the electric potentials and the electric charges respectively on the upper and lower faces of the piezoelectric beam (see Fig.2). The forces vector  $\mathbf{F}\mathbf{r}_b = (\mathbf{R}_A^x, \mathbf{R}_A^y, \mathbf{H}_A^z, \mathbf{R}_B^x, \mathbf{R}_B^y, \mathbf{H}_B^z)^t_{R_p}$  is due to the external mechanical work (see Fig.3).

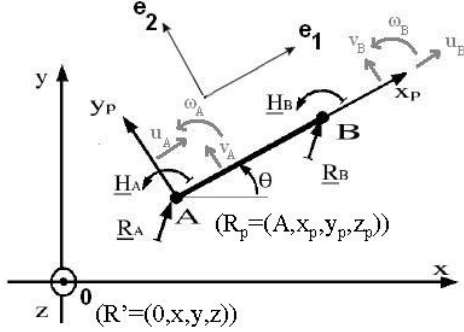


**Figure 3:** Curvilinear coordinates of the piezoelectric beam  $A - B$ , and its orientation in the global coordinate system  $R' = (0, x, y, z)$ .  $\mathbf{R}$  and  $\mathbf{H}$  represent the in-plane nodal force and moment at the beam extremities.

Corresponding matrices are expressed as follows:

$$\mathbf{M}_b = \rho A \begin{pmatrix} \frac{L}{3} & 0 & 0 & \frac{L}{6} & 0 & 0 \\ 0 & \frac{13L}{35} & \frac{11L^2}{210} & 0 & \frac{9L}{70} & -\frac{13L^2}{420} \\ 0 & \frac{11L^2}{210} & \frac{L^3}{105} & 0 & \frac{13L^2}{420} & -\frac{L^3}{140} \\ (sym.) & & & \frac{L}{3} & 0 & 0 \\ 0 & \frac{9L}{70} & \frac{13L^2}{420} & 0 & 0 & 0 \\ 0 & -\frac{13L^2}{420} & -\frac{L^3}{140} & 0 & 0 & \frac{L^3}{105} \end{pmatrix}_{R_p} \quad (2)$$

$$\mathbf{K}_b = Y \begin{pmatrix} \frac{A}{L} & 0 & 0 & -\frac{A}{L} & 0 & 0 \\ 0 & \frac{12I}{L^3} & \frac{6I}{L^2} & 0 & -\frac{12I}{L^3} & \frac{6I}{L^2} \\ 0 & \frac{6I}{L^2} & \frac{4I}{L} & 0 & -\frac{6I}{L^2} & \frac{2I}{L} \\ (sym.) & & & \frac{A}{L} & 0 & 0 \\ 0 & -\frac{12I}{L^3} & -\frac{6I}{L^2} & 0 & 0 & 0 \\ 0 & \frac{6I}{L^2} & \frac{2I}{L} & 0 & 0 & -\frac{4I}{L^2} \end{pmatrix}_{R_p} \quad (3)$$

$$\mathbf{G}_b = Y h d_{31} \begin{pmatrix} 1 & 0 & 0 & -1 & 0 & 0 \\ -1 & 0 & 0 & 1 & 0 & 0 \end{pmatrix}_{R_p}^t \quad (4)$$

$$\mathbf{C}_b = \frac{hL\tilde{\epsilon}_{33}}{e_p} \begin{pmatrix} 1 & -1 \\ -1 & 1 \end{pmatrix}_{R_p} \quad (5)$$

where  $I = \frac{e_p h^3}{12}$  is the inertia moment of the beam cross section  $A = e_p h$ ,  $\rho$  the density of the beam,  $Y$  its Young's modulus, and  $\tilde{\epsilon}_{33}$  its modified electric permittivity, function of the piezoelectric material properties.

The second equation in (1) represents the electric charges generated on the sensing beam electrodes via the direct effect of piezoelectricity. To measure these charges experimentally, charge-voltage converters are usually required using operational amplifier (see Fig.4). In ideal mode, upper and lower electrodes of the piezoelectric beam are considered to be shorted-circuit, so that zero-voltage  $\Phi_b$  is

applied in (1). This assumption ensures that sensing and actuation functions of piezoelectric beams are decoupled.

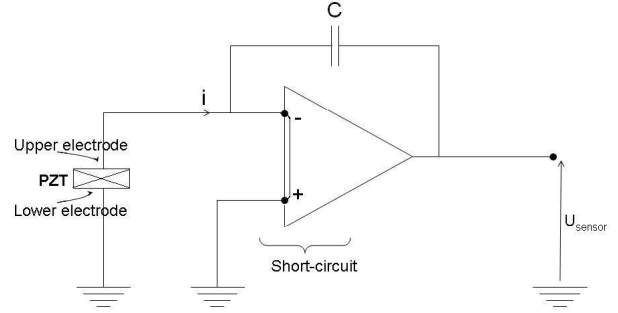


**Figure 4:** Basic electronic circuit for electric charges measurements based on charge-voltage converter.

## 2.2.2 FE model of piezoelectric structures

The piezoelectric blocks' matrices are calculated by the association of corresponding beam matrices in the global coordinate system of the structure. Each flexible structure is then defined as a finite-dimensional linear system modelled by:

$$\begin{aligned} \mathbf{M}_g \ddot{\eta}_g + \mathbf{K}_g \eta_g &= \mathbf{E}_g \mathbf{u} \\ \mathbf{y}_{co} &= \delta = \mathbf{F}_g \eta_g \\ \mathbf{y}_{ob} &= \mathbf{q}_g = \mathbf{L}_g \eta_g \end{aligned} \quad (6)$$

The foregoing second-order differential matrix equations represent the undamped dynamic behaviour of such a system, where  $\mathbf{M}_g$  and  $\mathbf{K}_g$  are the structure's mass and stiffness matrices respectively, obtained by the assembly of the matrices of all the blocks constituting the structure. Considering the integers  $p$ ,  $s$ , and  $r$ , as respectively the numbers of DOFs of the structure, number of inputs (i.e. actuators), and number of tip displacement outputs,  $\eta_g$  is then the  $p \times 1$  nodal displacement vector and  $\mathbf{u}$  is the  $s \times 1$  input vector. The  $p \times s$  input matrix  $\mathbf{E}_g$  reflects the location of the actuated DOFs, while  $\mathbf{y}_{co}$  is the  $r \times 1$  controlled output vector representing the output tip displacement  $\delta$  through  $r \times p$  output displacement matrix  $\mathbf{F}_g$ . The third equation expresses the electric charges ( $\mathbf{y}_{ob} = \mathbf{q}_g$ ) obtained by the integrated sensing function from the direct piezoelectric effect. It will serve as a static criterion maximizing the amount of sensing electric charges (see criterion  $J^2$  in section 4.1). Note that  $\mathbf{L}_g$  is the  $1 \times p$  single output matrix indicating the placement of piezoelectric sensor in the structure. Furthermore, it is important to note that controlled output variable ( $\mathbf{y}_{co}$ ) is not the observed output one ( $\mathbf{y}_{ob}$ ), as in usual other microrobotic systems, where the controlled tip of the piezocantilever is observed through external sensor.

### 3 A New Criterion for Matching Observability and High Control Authority Optimization

In order to successfully achieve suitable dynamic open-loop performances for further closed-loop control (see section 3.3), an optimal topology design strategy is derived taking into account control-observability criterion. The latter based on modal balanced gramians and observability gramians interpretations will be defined to help optimally integrating actuators and sensors in the microstructure. To do so, the physical coordinate base representation (6) is firstly transformed in the modal base to display the flexible modes. Then, we design an observer that will estimate the flexible modes included in the state vector through the measured electric charge vector  $\mathbf{q}_g$  on the sensing blocks of our optimal device. Finally we propose to control the output tip displacement  $\delta$  through a state feedback corrector.

#### 3.1 Modal representation of flexible structures

The harmonic solutions of the first equation in (6) give the eigenvectors matrix  $\Psi$  and natural frequencies  $\omega_i$  of the system. Details of the modal representation computation is given in [4]. We then obtain:

$$\begin{aligned} \ddot{\mathbf{z}} + \text{diag}(2\xi_i\omega_i)\dot{\mathbf{z}} + \text{diag}(\omega_i^2)\mathbf{z} &= \Psi^t \mathbf{E}_g \mathbf{u} \\ \mathbf{y}_{co} = \delta &= \mathbf{F}_g \Psi \mathbf{z} \\ \mathbf{y}_{ob} = \mathbf{q}_g &= \mathbf{L}_g \Psi \mathbf{z} \end{aligned} \quad (7)$$

where  $\mathbf{z}$  is the  $p \times 1$  modal displacement vector, and  $\xi_i$  is the  $i^{th}$  modal damping ratio introduced using Basil's hypothesis.

One interesting  $2p \times 1$  state vector  $\mathbf{x}$  typically used for flexible structures, and whose advantages are revealed in [10], consists of modal velocities and frequency-weighted modal displacements:

$$\mathbf{x} = \begin{pmatrix} \dot{z}_1 & \omega_1 z_1 & \dots & \dot{z}_p & \omega_p z_p \end{pmatrix}^t \quad (8)$$

Since controlled and observed output vectors are not the same, the modal state-space representation can be written as follows:

$$\begin{aligned} \dot{\mathbf{x}} &= \mathbf{A}\mathbf{x} + \mathbf{B}\mathbf{u}, \\ \mathbf{y}_{co} &= \mathbf{C}_{co}\mathbf{x}, \\ \mathbf{y}_{ob} &= \mathbf{C}_{ob}\mathbf{x}. \end{aligned} \quad (9)$$

which leads to two matrices triplets  $(\mathbf{A}, \mathbf{B}, \mathbf{C}_{co})$  and  $(\mathbf{A}, \mathbf{B}, \mathbf{C}_{ob})$  designating the control and observation state space models respectively.

The matrices take the forms  $\mathbf{A} = \text{diag}(\mathbf{A}_1, \dots, \mathbf{A}_p)$ ,  $\mathbf{B} = (\mathbf{B}_1^t, \dots, \mathbf{B}_p^t)^t$ ,  $\mathbf{C}_{co} = (\mathbf{C}_{co1}, \dots, \mathbf{C}_{cop})$ , and  $\mathbf{C}_{ob} = (\mathbf{C}_{ob1}, \dots, \mathbf{C}_{obp})$ , with, for  $i = 1, \dots, p$ ,

$$\mathbf{A}_i = \begin{bmatrix} -2\xi_i\omega_i & -\omega_i \\ \omega_i & 0 \end{bmatrix} \quad (10)$$

$$\mathbf{B}_i = \begin{bmatrix} \mathbf{b}_i \\ 0 \end{bmatrix} \quad (11)$$

$$\mathbf{C}_{coi} = \begin{bmatrix} 0 & \frac{\mathbf{c}_{coi}}{\omega_i} \end{bmatrix} \quad (12)$$

$$\mathbf{C}_{obi} = \begin{bmatrix} 0 & \frac{\mathbf{c}_{obi}}{\omega_i} \end{bmatrix} \quad (13)$$

where  $\mathbf{b}_i$ ,  $\mathbf{c}_{coi}$ , and  $\mathbf{c}_{obi}$  are the  $i^{th}$  components of  $\Psi^t \mathbf{E}_g$ ,  $\mathbf{F}_g \Psi$  and  $\mathbf{L}_g \Psi$  respectively. Matrix  $\mathbf{A}$  revolves around the structural parameters (eigen frequencies and damping ratio), whereas matrix  $\mathbf{B}$  depends on the location of actuated DOF, matrix  $\mathbf{C}_{co}$  on the location of desired displacement output, and matrix  $\mathbf{C}_{ob}$  on the location of integrated piezo-electric sensors. Fig. 5 shows the control-observation diagram principle to be applied at the end on our system.

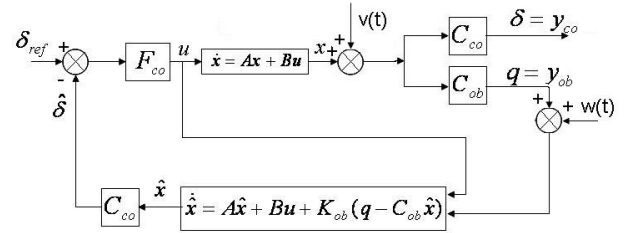


**Figure 5:** Control-observation diagram for compliant mechanism with integrated piezoactuator and piezosensor where  $F_{co}$  and  $K_{ob}$  are the control and observer gains respectively.

#### 3.2 Computation of the observability and balanced gramians

Observability gramian ( $\mathbf{W}_{ob}$ ) between state  $\mathbf{x}$  and measured output  $\mathbf{q}_g$  is found to be convenient to characterize the modes' observability by the mean of electric charge  $\mathbf{q}_g$ . Its energetic and geometric interpretations are demonstrated in [5] and [11]. For stable  $\mathbf{A}$ ,  $\mathbf{W}_{ob}$  is obtained from algebraic solution of following Lyapunov equation:

$$\mathbf{A}^t \mathbf{W}_{ob} + \mathbf{W}_{ob} \mathbf{A} + \mathbf{C}_{ob}^t \mathbf{C}_{ob} = 0 \quad (14)$$

Assuming that the damping ratios are infinitely small and the natural frequencies well spaced, which is widely accepted for flexible structures, the block diagonal forms of  $(\mathbf{A}, \mathbf{C}_{ob})$  couple can be exploited to give closed-form analytical solution for the expression of the modal observability gramian [12]. It is diagonal and equal to:

$$\mathbf{W}_{ob} = \text{diag}(\mathbf{W}_{ob11}, \dots, \mathbf{W}_{obpp}) \quad (15)$$

with, for  $i = 1, \dots, p$ ,

$$\mathbf{W}_{obi} = \frac{\gamma_{qii}}{4\xi_i\omega_i^3} \mathbf{I}_2 = \alpha_i \mathbf{I}_2 \quad (16)$$

where  $\gamma_{qii} = \mathbf{c}_{obi}^t \mathbf{c}_{obi}$ , and  $\mathbf{I}_2$  is the  $2 \times 2$  identity matrix. For a given mode  $(\xi_i, \omega_i)$ ,  $\gamma_{qii}$  scalars represent the



way the  $i^{th}$  mode is seen through the piezoelectric sensor blocks.

On the other hand, the observer should be able to reconstruct the dominant modes of  $\delta/u$  transfer by measuring  $\mathbf{q}_g$  (see Fig. 6). These dominant modes are symbolized by high Hankel singular values (HSVs) defining the balanced gramian  $\mathbf{W}_{e\delta}$  of  $(\mathbf{A}, \mathbf{B}, \mathbf{C}_{co})$  system as follows:

$$\mathbf{W}_{c\delta} = \mathbf{W}_{o\delta} = \mathbf{W}_{e\delta} = \text{diag}(\sigma_i) \quad (17)$$

where  $\sigma_i$  are the HSVs of the  $(\mathbf{A}, \mathbf{B}, \mathbf{C}_{co})$  system.

Note that balanced gramian is a useful tool for quantifying the joint controllability and observability of the system. It is shown that when the damping ratios decrease to zero, the physical modal state coordinates are approximately balanced in this asymptotic situation, and the approximate  $i^{th}$  Hankel singular value for flexible structure is given by [12]

$$\sigma_i = \frac{\sqrt{\mathbf{c}_{coi}^t \mathbf{c}_{coi} \mathbf{b}_i \mathbf{b}_i^t}}{4\xi_i \omega_i^2} \quad (18)$$

HSV describes the degree of the corresponding modal state's input-output energy flow through the system.

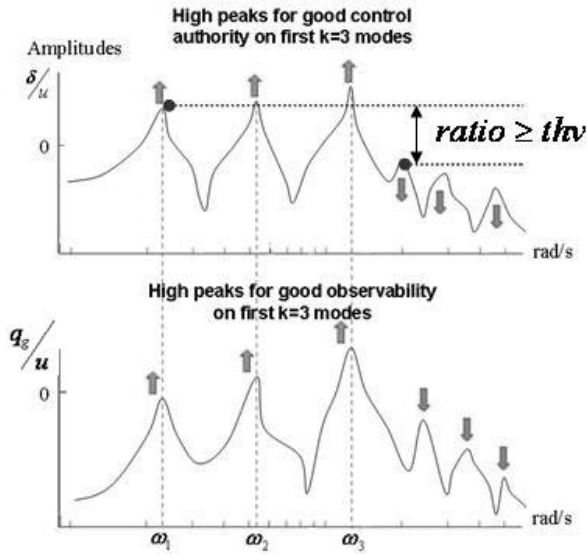


**Figure 6:** Example of desired form of Control and Observation transfers.

### 3.3 A gramian-based criterion for optimal placement of piezoelectric sensor within a piezoelectric microactuator

Considering the statements made in Section 3.2, this kind of active structures which are to be finely controlled are confronted with two main issues:

1) A reduced model of the structure must be developed, which includes the few dominant low frequency modes,

without destabilizing the system by rejecting the residual modes (i.e. high roll-off after the dominant modes).

2) If the dominant modes are not all observed, the reconstruction of  $\hat{\delta}$  will not be guaranteed in an optimal way by the observer.

As mentioned earlier, each piezostructure suggested in the optimization procedure is evaluated according to the specified criteria. Hence, we developed a new criterion to help overcome these two difficulties: the first problem is overcome by forcing the optimal structure to have  $k$  first dominant modes of the  $\delta/u$  transfer in order to reduce the model without the residual modes affecting it. Then, to surmount the second problem, we guarantee a high-level of observability of these dominant modes by means of electric charge  $\mathbf{q}_g$ . It is thus presented by a procedure formulated as follows:

$$\text{If } \frac{\sigma_{i=1 \rightarrow k}^{min}}{\sigma_{j=k+1 \rightarrow p}^{max}} \geq thv, \quad (19)$$

$$\text{then } \mathbf{J}^{k,n,thv} = \frac{\sigma_{i=1 \rightarrow k}^{min}}{\sigma_{j=k+1 \rightarrow p}^{max}} \cdot \sum_{i=1}^k \alpha_i \left( \frac{\sigma_i}{\sigma_{j=1 \rightarrow k}^{max}} \right)^n \quad (20)$$

where  $k$  is the number of the first dominant modes specified by the designer,  $\sigma_{i=1 \rightarrow k}^{min}$  and  $\sigma_{j=k+1 \rightarrow p}^{max}$  are respectively the level of the least dominant mode within the first  $k$  and the level of the most dominant mode within the residual ones.  $thv$  is a threshold value specified by the designer. Hence, the condition (19) represents the domination of the  $k$  first modes by at least  $thv$  times compared to the residual modes (see Fig. 6). Furthermore, in the numerical expression (20) of the criterion itself,  $\alpha_i = \frac{\gamma_{q_{ii}}}{4\xi_i \omega_i^3}$  corresponds to the coefficient of the  $i^{th}$  observability modal gramian  $\mathbf{W}_{ob_{ii}} \cdot \left( \sigma_i / \sigma_j^{Max} \right)^n$  is a weighing ratio  $\in [0, 1]$ . When the latter's value is close to 1, the  $i^{th}$  mode in question is a dominant mode within the first  $k$  ones. Note that the exponent  $n$  helps emphasizing the most dominant modes by accelerating the convergence towards  $\sigma_i^{Max}$ . Thus, the corresponding  $\alpha_i$  is privileged compared to other modes' observability. In other words, by maximizing this criterion, we privilege the modes where good observability of  $\delta$  coincides with its dominant modes (Fig. 6). In this way, it appears that the procedure given by (19) and (20) is able to solve the problems mentioned above.

## 4 Optimal Synthesis of Monolithic Piezoelectric Mechanism with Integrated Actuator and Sensor

### 4.1 Optimization problem specifications

We consider here the optimal synthesis of a monolithic micromechanism with integrated actuator and sensor, made of the piezoelectric material PIC151 from PI Piezo Ceramic Technology [13].

The structure is considered to have a maximal size of  $15\text{mm} \times 18\text{mm}$ , and a constant thickness of  $200\mu\text{m}$ . It is defined to be made of either, passive, active or sensitive blocks inside a  $2 \times 3$  mesh (see Fig. 7). For the optimal synthesis run, the number of active (resp. sensitive) blocks in the structure, chosen among blocks given in Fig. 1, will be allowed to vary between 1 and 4. The size ratio of the blocks can vary as  $b_{\max}/b_{\min} \in [1; 2]$  and  $a_{\max}/a_{\min} \in [1; 2]$  (see Fig. 7 for details about  $a$  and  $b$  parameters definitions). When external voltages are applied to the actuating blocks' electrodes, the chosen output node of the structure has to move along the  $x$ -axis (see Fig. 7). For evaluation of static mechanical criteria, the potential difference between upper and lower face is taken equal to  $200\text{V}$ . The number of blocked nodes is comprised between 1 and 3 among the locations permitted, which are reported in Fig. 7.

Finally, three numerical criteria to be maximized simultaneously with FlexIn are:

- $J^1$ : free mechanical displacement  $\delta_x$  at the output node in  $x$ -direction,
- $J^2$ : amplitude of the sensing electric charges induced on the piezoelectric blocks, numerically computed by means of the third equation in (6),
- $J^{k,n,thv}$ : modal observability of the mechanism output  $\delta$  by the observed sensitive blocks charges  $\mathbf{q}_g$ . In this example, we chose  $k = 2$ ,  $n = 2$  and  $thv = 3$ .

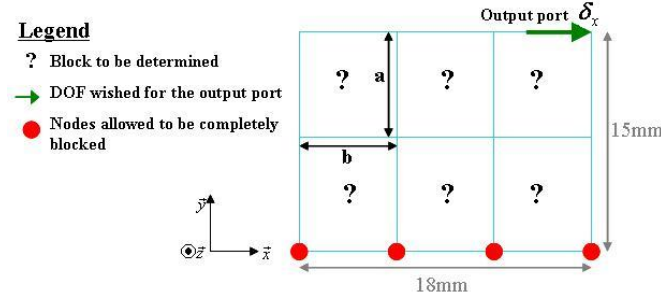


**Figure 7:** Mesh of the PZT compliant micromechanism with imposed and permitted boundary conditions.  $a$  and  $b$  optimization parameters define the relative height and width of the blocks.

## 4.2 Results and performances comparison

After setting the optimization to run, if during 200 subsequent generations, the genetic algorithm does not find new pseudo-optimal solutions, the optimization procedure is automatically stopped, resulting into Pareto fronts such as in Fig. 8, showing the best compromises kept. From these fronts, the designer can choose the structure that is most appropriate to his study. In our case, performances of three selected pseudo-optimal solutions are compared in Fig. 9.

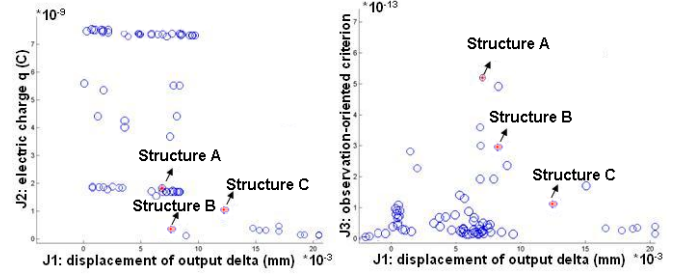


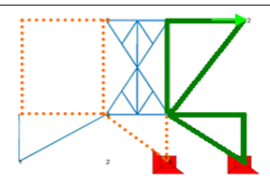
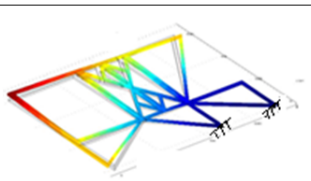
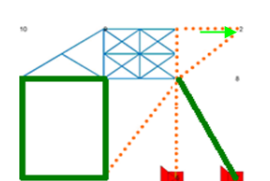
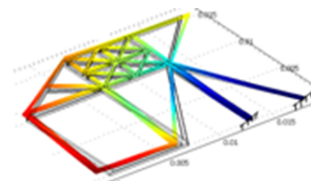
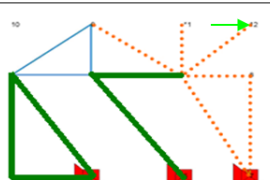
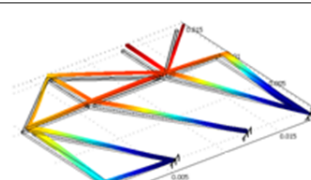
**Figure 8:** Pareto fronts of compliant mechanisms synthesized using FlexIn.

Structure C exhibits the best output displacement (highest  $J^1$  value), whereas structure A has the best dynamic characteristics (highest  $J^{k,n,thv}$  value). As for  $J^2$  criterion, it is found to be essential in increasing the range of electric charges induced on the piezoelectric sensor parts, for quasi-static measurements. In fact, in the latter mode, electric charges less than  $10^{-9}\text{C}$  require special electronic circuits, because they desert the sensor surface as soon as they are generated. Hence, even though the structures selected do not have the best  $J^2$  values among all the pseudo optimums, structures A and C present measurable charges quantities, via circuits based on charge-voltage converters as mentioned in section 2.2.1.

To illustrate the dynamic performances, bode diagrams of control and observation transfers of the three structures are presented in Fig. 10. The control authority of the first  $k = 2$  selected modes in the three structures is properly insured by the criterion condition (19), as shown in Fig. 10.a. As for  $J^{k,n,thv}$  value itself presented by (20), it symbolizes significantly the same modes' observability. In fact, as expected, structure C has the poorest observability, demonstrated by a small peak in the amplitude of the observation transfer  $\mathbf{q}_g/\mathbf{u}$  of the second mode (see Fig. 10.b). For a greater value of  $J^{k,n,thv}$ , structure B shows better observability of the first two modes. One problem remains: the existence of the first anti-resonance complicates the computation of modal representation and thus the control of such structure via a state observer. Finally, structure A having the highest  $J^{k,n,thv}$  value, it exhibits ideal observability of the first two modes, as reported by the high amplitude peaks of  $\mathbf{q}_g/\mathbf{u}$  transfer (see Fig. 10.b).

## 5 Conclusion

A contribution to an existing optimal compliant micromechanisms design method has been presented in this paper. In this method, structures monolithically machined, composed of an assembly of building blocks made of PZT, optimally integrate actuating and sensing blocks by means of two new criteria: first, a static one, maximizing the amount of electric charges induced on the sensor surfaces via the direct piezoelectric effect; the second one is a control-observation oriented gramian-based criterion, considering the open-loop dynamic control and observation transfers' performances of the structure.

Structure	FlexIn Scheme	Comsol Scheme	$J^1$ ( $\mu\text{m}$ )	$J^2$ ( $10^{-9}$ C)	$J^{k,n,thv}$ ( $10^{-13}$ )
A			7	1.91	5.1
B			7.78	0.25	1.83
C			12.34	1.01	0.94

Passive blocks  
Active blocks  
Sensitive blocks

**Figure 9:** FlexIn representation, 3D commercial simulation software representation and performances of the A, B and C compliant structures.

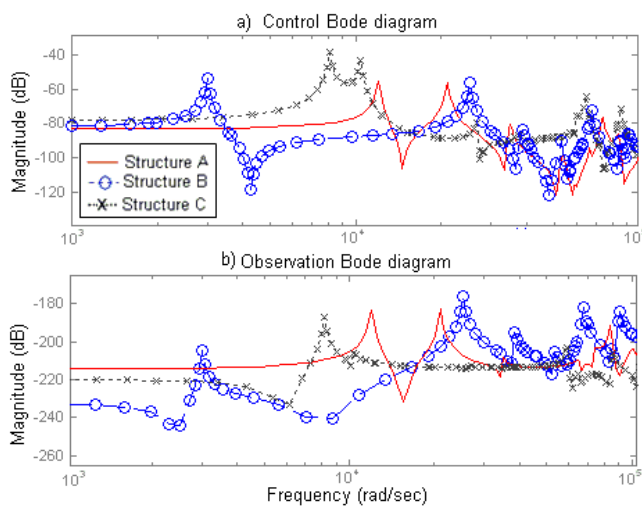


**Figure 10:** Frequency responses of A, B and C structures of a) control transfer  $\delta/u$  and b) observation transfer  $q_g/u$ .

In fact, for optimally integrating both actuation and sensing functions in the structure, the second criterion implies matching high control authority modes from the balanced gramian matrix, with high observation ability from the observation gramian matrix.

An optimization problem is specified to illustrate the mentioned methodology. The analysis of three resulting pseudo-optimal solutions brings to satisfying conclusion: the structures have good static characteristics due to  $J^1$  and

$J^2$  criteria, but more importantly, a high value of  $J^{k,n,thv}$  insures good observability of the selected dominant modes. This successfully sought property will simplify the control of such structures via state observer. A prototype of the compliant pseudo-optimal micromechanism, structure A, will be developed for experimental validations and control.

## References

- [1] Lin, X.; Yuan, F.G.: *Diagnostic lamb waves in an integrated piezoelectric sensor/actuator plate: analytical and experimental studies*, Smart Materials and Structures 10. 2001, pp 907-913
- [2] Campolo, D.; Sahai, R.; Fearing, R.S.: *Development of piezoelectric bending actuators with embedded piezoelectric sensors for micromechanical flapping mechanisms*, IEEE Int. Conf. on Robotics and Automation. Taiwan: Taipei, 2003, pp 3339-3346
- [3] Silva, E.C.N.; Kikuchi, N.: *Design of piezoelectric transducers using topology optimization*, Smart Material and Structures. Vol. 8, 1999, pp 350 -365
- [4] Grossard, M.; Rotinat-Libersa, C.; Chaillet, N.; Boukallel, M.: *Mechanical and control-oriented design of a monolithic microgripper using a new topological optimization method*, IEEE/ASME Transactions on Mechatronics. Vol. 14, No. 1, 2009, pp 32-45
- [5] Leleu, S.; Abou-Kandil, H.; Bonnassieux, Y.: *Piezoelectric Actuators and Sensors Location for Active*

*Control of Flexible Structures*, IEEE Trans. on Instrumentation and Measurement. Vol. 50, No.6, 2001, pp 1577-1582

- [6] Collet, M.; Jezequel, L.: *Active modal control with piezoelectric layers optimisation*, Journal of Structural Control. Vol.1, issue 1-2, 1994, pp 59-77
- [7] Han, J.H.; Lee, I.: *Optimal placement of piezoelectric sensors and actuators for vibration control of composite plate using genetic algorithms*. Smart Materials and Structures 8, 1999, pp 257-267
- [8] Bernardoni, P.; Bidaud, P.; Bidard, C.; Gosselin, F.: *A new compliant mechanism design methodology based on flexible building blocks*, Smart Material and Structures. Vol. 5383, USA, 2004, pp 244-254
- [9] Preumont, A.: *Mechatronics: Dynamics of Electromechanical and Piezoelectric Systems (Solid Mechanics and Its Applications)*, NewYork, Springer-Verlag, 2006.
- [10] Hac, A.; Liu, L.: *Sensor and actuator location in motion control of flexible structures*, J. Sound Vib. Vol. 167, No. 2, 1993, pp 239-261
- [11] Jonckheere, E. A.: *Principal components analysis of flexible systems, Open-loop case*, IEEE Trans. Autom. Control. Vol. AC-29, No. 12, 1984, pp 1095-1097
- [12] Gawronski, W.; Lim, K. B.: *Balanced Control of Flexible Structures*, London, U.K. Springer-Verlag, 1996
- [13] PI Piezo Ceramic Technology, Available at: <http://www.piceramic.com/>.